Synthesis and Characterization of New Ceramic Thermoelectrics Implemented in a Thermoelectric Oxide Module

P. TOMEŠ,[1] R. ROBERT,[1] M. TROTTMANN,[1] L. BOCHER,[1]
M.H. AGUIRRE,[1] A. BITSCHI,[2] J. HEJTMÁNEK,[3] and A. WEIDENKAFF[1,4]

1.—Solid State Chemistry and Catalysis, Empa, Swiss Federal Laboratories for Materials Testing and Research, Ueberlandstrasse 129, CH-8600 Duebendorf, Switzerland. 2.—High Voltage Laboratory, Swiss Federal Institute of Technology, Physikstrasse 3, 8092 Zurich, Switzerland. 3.—Institute of Physics of ASCR, v.v.i, Na Slovance 2, 182 21 Praha 8, Czech Republic. 4.—e-mail: anke.weidenkaff@empa.ch

Novel thermoelectric oxides were developed, produced, and characterized to demonstrate their promising thermoelectric conversion potential in a thermoelectric converter. Four-leg thermoelectric oxide modules were fabricated by combining p- and n-type oxide thermoelements made of pressed polycrystalline $GdCo_{0.95}Ni_{0.05}O_3$ and $CaMn_{0.98}Nb_{0.02}O_3$, respectively. In these modules, the p- and n-type thermoelements were connected electrically in series and thermally in parallel. The materials were joined by electrical contacts consisting of a Ag/CuO composite material. Fairly good thermal contacts were ensured by pressing the thermoelements between alumina substrates. Cross-sections of the alumina/Ag–CuO mixture/thermoelement interface were investigated by scanning electron microscopy. The temperature distribution across the module was monitored using K-type thermocouples and a micro-infrared (IR) camera. The open-circuit voltage and the load voltages of the module were measured up to a temperature difference of $\Delta T = 500$ K while keeping the temperature of the cold side at 300 K. The output power and internal resistance were calculated. The characteristics of the module evaluated from electrical measurements were compared with respective values of the p- and n-type leg materials. An output power of 0.04 W at $\Delta T = 500$ K led to a power density of $\sim$0.125 W/cm^3, where the volume of thermoelectric material was determined by a cross-section of 4 mm $\times$ 4 mm and a leg length of 5 mm.

Key words: Thermoelectric materials, perovskites, power generation, oxide ceramics, micro-IR camera measurement

INTRODUCTION

The foreseeable decline of fossil-fuel resources is promoting growing interest in renewable energy technologies such as solar energy converters and heat recovery techniques. The manufacturing industry, automobiles, and thermal power plants lose a lot of energy to heat, which could be recovered and converted to electricity by a new generation of improved thermoelectric (TE) devices. TE converters directly convert this heat into electricity. The advantage of thermoelectric modules compared with mechanical or chemical energy conversion technologies such as Stirling engines, Rankine cycles, and solid oxide fuel cells (SOFC)[1] is that they do not involve moving parts and operate unfueled. Therefore, low-maintenance TE modules rank among the most promising energy conversion technologies. The thermoelectric performance of a TE material is defined by the figure of merit, $ZT = S^2T/\rho\kappa$, where S is the Seebeck coefficient, ρ is the electrical resistivity, and κ is the thermal

conductivity. The efficient conversion of heat into electricity requires thermoelectric materials with a high figure of merit and long-term stability. Thus, the material should be inert and have a large Seebeck coefficient, low resistivity, and low thermal conductivity. Conventional thermoelectric modules based on Bi_2Te_3[2] exhibit relatively high conversion efficiencies but limited temperature stability in air. On this account, TE research during the last decade has focused on environmentally friendly new complex metal oxides,[3–7] because of their good thermal stability in air, cost-efficient production processes, and excellent thermomechanical properties. The large Seebeck coefficients coupled with relatively good electrical transport properties relies on a recently discovered spin–orbit entropy factor.[8] These unconventional but promising thermoelectric materials have been less extensively studied compared with well-known Bi_2Te_3-type thermoelectrics. The performance of these new functional materials based on complex metal oxides will be demonstrated in a real energy conversion process.

Here we report on the preparation of matching p- and n-type oxide thermoelectric materials for a four-leg thermoelectric oxide module (TOM) for potential future application in high-temperature thermoelectric devices.[9–12] The TE performance of the modules has been validated by measurement of the output power and open-circuit voltage, and by evaluation of the internal resistance. The quality of the electrical and thermal contacts is assessed, which plays an important role in optimization of module performance. Therefore, composite materials are chosen which minimize heat and electrical losses and also ensure mechanical stability.

An accurate temperature gradient measurement along the legs is crucial since this is an important parameter to calculate the output power. Therefore, micro-IR camera measurements have been conducted in order to precisely evaluate the temperature distribution along the p- and n-type legs and at the Al_2O_3–Ag/CuO–p-/n-type leg interfaces.

EXPERIMENTAL PROCEDURES

Powders of p-type $GdCo_{0.95}Ni_{0.05}O_3$[13] and n-type $CaMn_{0.98}Nb_{0.02}O_3$[14] thermoelectric materials were synthesised by *chimie douce*[15,16] processes based on chelation of metal cations with citric acid in aqueous solution. The citrate precursor solutions were prepared by dissolving the required amounts of $Ca(NO_3)_2 \cdot 4H_2O$ (Fluka, ≥99%), $Gd(NO_3)_3 \cdot 6H_2O$ (Merck, ≥97%), $Mn(NO_3)_2 \cdot 4H_2O$ (Merck, >98.5%), and $Ni(NO_3)_2 \cdot 6H_2O$ (Merck, ≥99%) in deionized water. $NbCl_5$ (Aldrich, >99.5%) was dissolved in hydrochloric acid before adding it to the solution. Citric acid ($C_6H_8O_7$, Riedel-de Häen, >99.5%) was added in excess (citric acid/metal cations molar ratio of CA/M = 2/1) in order to prevent precipitation and hydrolysis of $NbCl_5$. The precursor solutions were homogenized and polymerized at 353 K for 3 h

under continuous stirring. No precipitation was observed, which indicates the formation of water-soluble polymeric complex compounds. The xerogel precursors were heated in air to 573 K with a heating rate of 20 K/min and predecomposed for 3 h at this temperature. After intermediate grinding, the cobaltate and manganate ash-like powders were calcined at 1073 K and 1173 K for 6 h, respectively. X-ray diffraction analysis (XRD) was used to confirm single-phase purity. Final products were pressed into bar-shaped pellets of 25 mm × 5 mm × 5 mm. The cobaltate and manganate pellets were sintered for 6 h at 1373 K and at 1523 K, respectively. The pellets contracted during sintering and were subsequently cut into ∼5 mm × 4 mm × 4 mm legs for the TOM.

Electrical resistivities and Seebeck coefficients were measured by using a RZ2001i Ozawa Science unit in the temperature range of 300 K to 800 K in air. The reproducibility of the values was very high, with an error in the range of 3% to 5%. The equipment was calibrated by using standard materials (e.g., Ni, PbTe, Ca349) from round-robin tests and confirmed by other physical property analysis systems such as an in-house manufactured Seebeck measurement device. The high-temperature thermal conductivity was determined from separate measurements of thermal diffusivity and heat capacity using a Netzsch LFA 457 laser flash apparatus and a Netzsch DSC 404 C Pegasus apparatus, respectively. Comprehensive ongoing error estimations of the thermal conductivity measurements consider inhomogeneous porosities and real structures of the material in contrast to 100% dense materials and calculated materials constants.

The resulting four-leg thermoelectric oxide module consisted of two pairs of p- and n-type legs (Fig. 1). The thermoelectric legs had a cross-sectional area of 4 mm × 4 mm and length (height) of 5 mm. The n-type $CaMn_{0.98}Nb_{0.02}O_3$ and the p-type $GdCo_{0.95}Ni_{0.05}O_3$ thermoelements were connected electrically in series and thermally in parallel. The thermoelectric elements were placed between two thin Al_2O_3 layers with a thickness of 0.25 mm and area of 30 mm × 30 mm, which served as electrically
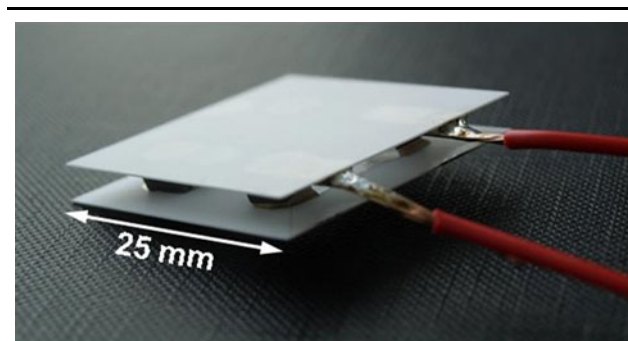

Fig. 1. Photo of a four-leg thermoelectric oxide module.

insulating and thermally conducting substrates for both the cold and the hot side of the module.

Different electric contacts, soldering and joining materials were tested in wetting experiments. Electrical contacts consisted of a mixture of Ag and CuO powders (e.g. 2 wt.% CuO for n-type, 0.5 wt.% CuO for p-type), which was pressed into disc-shaped pellets and annealed at T = 1193 K for several hours. After the thermal treatment, the Ag/CuO discs were further pressed by using a hydraulic press and polished to obtain the final metal foil with an approximate thickness of 150 μm. The foil was used to establish electrical contact between the ceramic legs and the Al_2O_3 substrates. Pellets of thermoelectric materials were covered with the electrical contact material and annealed in air up to 1243 K with a dwell time of 10 min. Finally, the thermoelectric legs were electrically connected in series by silver paste. The cross-section of the Al_2O_3–Ag/CuO-p- and n-type leg joint was studied with a Hitachi S-4800 scanning electron microscope (SEM) in order to examine the quality of the bonding in detail.

A test setup for the electrical and power measurements was mounted as shown in Fig. 2a. The testing apparatus consisted of: (1) a pressure device to control the pressure on the top side of the module and the heat transfer from the heater to the module, (2) a high-accuracy control unit to adjust the interfacial area between the heat source and the TOM surface, (3) a controllable electric heating plate to heat the upper side of the TOM, and (4) a copper block cooling part with circulating cold water to cool the bottom side of the TOM. The pressure load on the module during the test was ~2 N cm^{-2}.

A heat-conductive paste was applied between the thermal sink and the alumina plates of the module to improve heat transfer. K-type thermocouples were placed directly between the heating plate and Al_2O_3 layer on the hot side of the module and between the Cu cooling block and the Al_2O_3 layer on the cold side of the module, respectively, to measure the temperature gradient along the TE legs (Fig. 4a). Connection of the thermocouples was ensured by pressure contacts. Additional thermocouples were used to control the temperature of the heat source and the cooling water.

The output power at different loads was measured using automated parallel switching of four resistances by means of low-resistance relays. This configuration enables ten highly precise loads (R_{load}) to be applied. The voltage was examined in open-circuit mode (V_{OC}) and at load resistances by using a precise digital multimeter (DMM). The measurement was monitored and recorded by a LABVIEW applet running on a desktop computer. The internal resistance R_{in} was calculated using the relation

$$R_{in} = R_{load}[(V_{OC} - V_{load})/V_{load}]. \tag{1}$$

The maximum output power (P_{max}) for various loads related to different load voltages was calculated by using the general relation

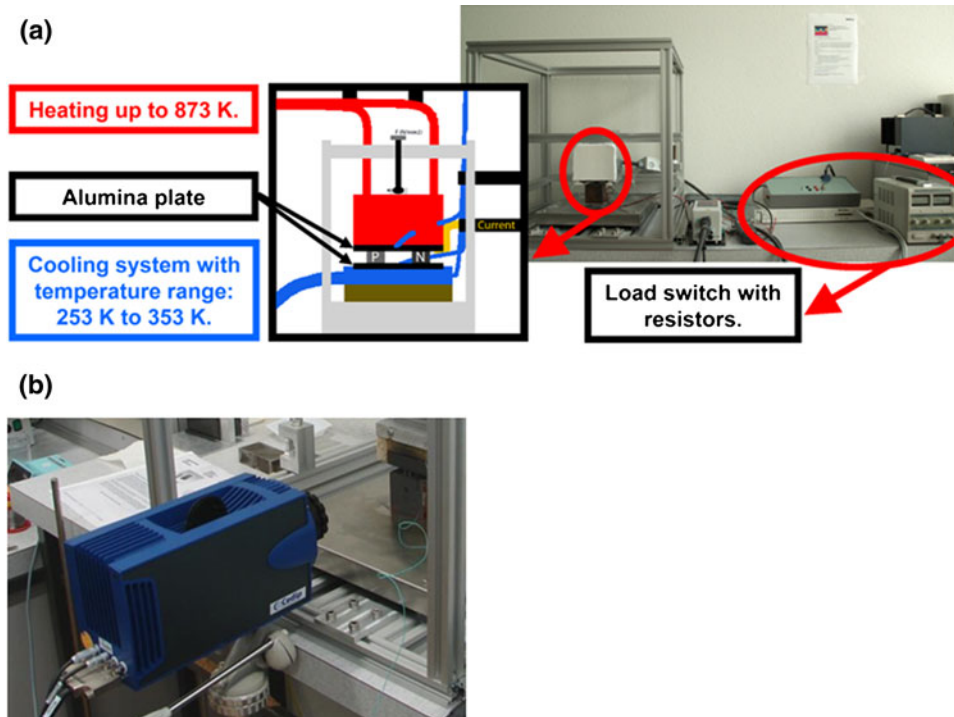$$P_{max} = V_{OC}^2/[4R_{load}((V_{OC} - V_{load})/V_{load})]. \tag{2}$$

Fig. 2. (a) Configuration of the electrical and power measurements setup and (b) of the micro-infrared (IR) camera (f = 50 mm and a 10 mm extension ring) for temperature profile measurements.

Detailed information about the temperature distribution along the legs (temperature gradient) of the module was obtained by measuring the reflection of the module surface using a micro-IR camera (Jade III for microthermographic measurements, from Cedip Infrared Systems; Fig. 2b). The InSb detector array of the camera has a resolution of 240×320 pixels and is sensitive to infrared radiation with wavelengths in the range of 3.6 μm to 5.0 μm. Dynamic measurements were performed with a frame rate of 10 Hz for the defined temperature gradient. A graphite spray was used to homogenize the surface emissivity of the samples. Data were evaluated using the IR-camera software.

RESULTS

Several batches of 50 g p-type $(GdCo_{0.95}Ni_{0.05}O_3)$ and n-type $(CaMn_{0.98}Nb_{0.02}O_3)$ powder materials were prepared in a highly reproducible synthesis process. Different complementary solid-state chemical analyses results (XRD, SEM, etc.) revealed single-phase products with particle size between 2 μm and 8 μm. These powders were processed into highly dense thermoelectric legs ($\sim$80% of theoretical density). Prior to assembly of the module, microscopic quality control ensured that only legs without fissures, flaws, and cracks were selected.

In Fig. 3a, b, the thermoelectric properties (S, ρ, and κ) of the n- and p-type materials are shown. The total thermal conductivity (κ) of both materials is close to 3 $Wm^{-1} K^{-1}$ above 300 K. Assuming that the Wiedemann–Franz law is valid, it can be

concluded that the dominant contribution to the thermal conductivity arises from the phononic part. Thus, a slight decrease of the thermal conductivity with increasing temperature is observed for both p- and n-type materials, suggesting Umklapp-process-mediated scattering of phonons. The thermal conductivity of the p-leg increases by 50% between $\sim$600 K and 800 K. This increase can be attributed to an increase of the electronic part of the thermal conductivity (κ_e). At 800 K, κ_e amounts to $\sim$0.54 $Wm^{-1} K^{-1}$, which represents $\sim$20% of the total thermal conductivity. The n-type leg shows an electronic contribution of $\sim$0.06 $Wm^{-1} K^{-1}$ at the same temperature, which is 3.4% of the total thermal conductivity.

The electrical resistivity (ρ) of the n-type leg (Fig. 3a) increases with increasing temperature, indicating metal-like behavior, whereas the p-type material (Fig. 3b) exhibits semiconducting-like behavior, i.e., the resistivity decreases with increasing temperature $d\rho/dT < 0$. The maximum output power is limited by the high electrical resistivity below 600 K of the p-type leg, leading to a high total internal resistance of the module.

Both compounds show large thermopower (S), confirming their potential as thermoelements. It has to be noted that the thermopower decrease of the p-type material (Fig. 3b) is related to the Co spin-state transition occurring at around 600 K.[17] The monotonic decrease of the thermopower together with the "metal-like resistivity" of the n-type material can be explained by a narrow-band model of e_g electrons.[18]
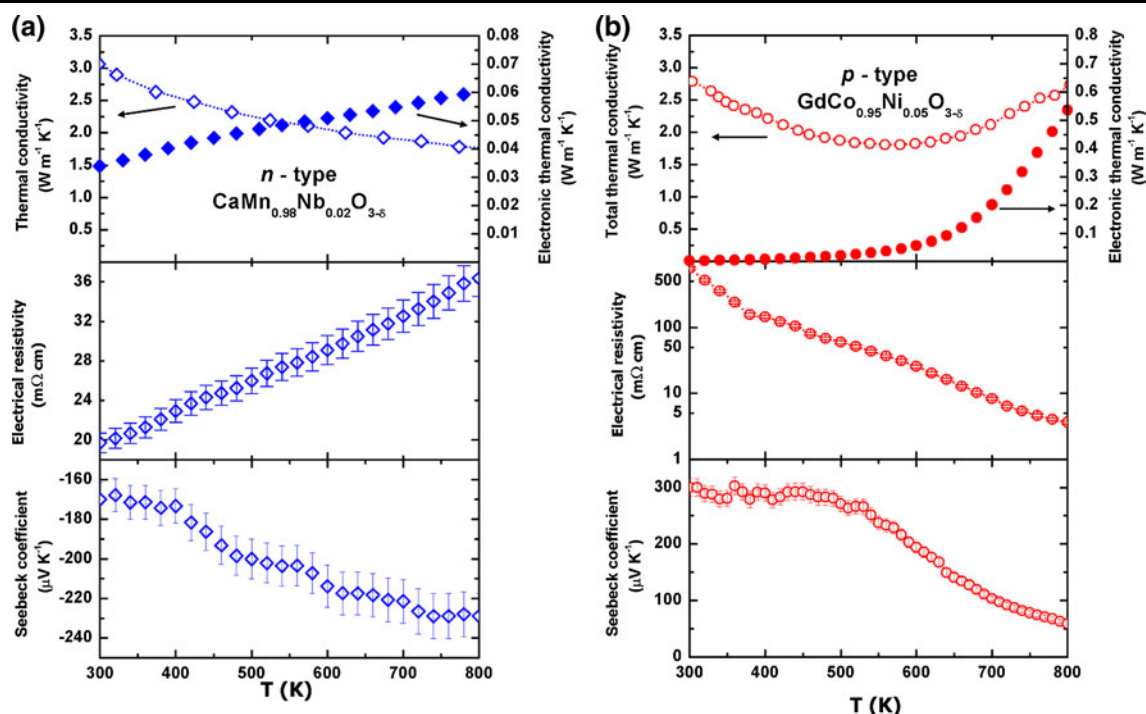

Fig. 3. (a) Temperature dependence of the thermoelectric properties (S, σ, and κ) of n-type $CaMn_{0.98}Nb_{0.02}O_{3-\delta}$ and (b) p-type $GdCo_{0.95}Ni_{0.05}O_{3-\delta}$.
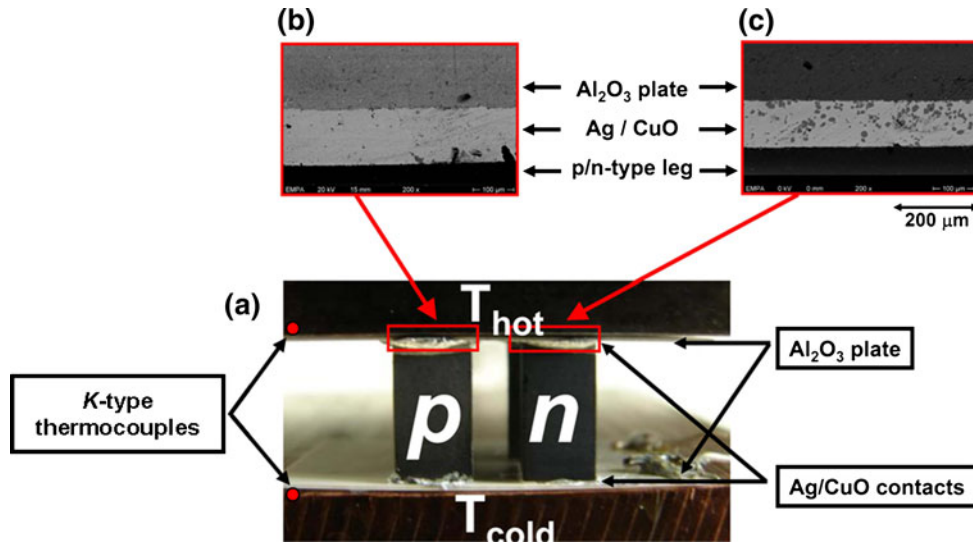
Fig. 4. (a) Cross-section SEM picture of the TOM, (b) detail of the Al_2O_3–Ag/CuO–$GdCo_{0.95}Ni_{0.05}O_3$ cross-section, and (c) detail of the Al_2O_3–Ag/CuO–$CaMn_{0.98}Nb_{0.02}O_3$ cross section.

A TE converter consists of a heat exchanger, thermal and electrical connections, and thermoelectric legs. The bonding process of the different components is crucial for the performance of the converter as well as for the mechanical and chemical interaction between the materials. The bonding material should provide sufficient mechanical connection and good electrical conductivity. It was found in several tests that the ductility of the bonding material based on a metal paste improves the overall mechanical properties. The electrical contacts must not increase the total resistance of the TE module and must simultaneously allow efficient heat transfer between source and TE legs. The electrical connection is separated in two regions and was therefore prepared in two steps. First, mixtures of Ag/0.5 wt.% CuO for $GdCo_{0.95}Ni_{0.05}O_3$ and of Ag/2 wt.% CuO for $CaMn_{0.98}Nb_{0.02}O_3$ with a high melting point (1243 K) were used to connect the TE legs to the Al_2O_3 substrate. In our case, the thickness of this contact layer was chosen to be around 150 μm. This is a good compromise between low resistance of the contact layer, good mechanical bonding (which is especially important under high thermal stress), and reliable operation of the TE modules. Second, additive-free Ag paste with a lower melting point (1193 K) was used to establish the 100-μm-thick electrical connection between the p- and n-type TE legs.

This two-step process was necessary to ensure sufficient mechanical stability of the TOM and to avoid any remelting of the Ag paste. The creation of the electrical contacts in a one-step process using only pure Ag paste increased the (contact) resistance by up to 0.25 Ω after three thermal operation cycles. Further temperature cycles broke the connection between the TE legs and the Al_2O_3 substrate.

In order to build a strong and reliable module with improved bonding and minimal interfacial stress as well as matching thermal expansion coefficients, a composite material with optimized composition was developed and tested in wetting and bonding experiments. The shape and contact angle θ of a droplet of molten braze filler material on a ceramic surface is determined by the balance of interacting forces (surface tensions) at the solid–vapor (γ_{sv}), solid–liquid (γ_{sl}), and liquid–vapor (γ_{lv}) interfaces. Accordingly, the wetting ability of a liquid is evaluated by Young's equation[19]:

$$\cos\theta = (\gamma_{sv} - \gamma_{sl})/\gamma_{lv}. \tag{3}$$

Good working connections and interfaces between the converter components (Al_2O_3 substrate and the thermoelectric legs) were achieved by using a suitable composite material, i.e., silver powder mixed with metal oxide particles. This silver-based joining technique with oxide additives was superior in terms of both wettability and joint strength of the resulting braze on polycrystalline alumina substrates[20] compared with pure silver contacts. Pure silver paste resulted in low wettability, and the contacts were droplet shaped with a contact angle of 114°.[21] By adding CuO, the contact angle decreased from 114° to 75°, showing an optimum at low CuO concentrations due to the formation of a homogeneous silver-copper oxide liquid. The test results revealed that the mechanical strength of the contacts was optimal when a mixture of Ag/0.5 wt.% CuO for $GdCo_{0.95}Ni_{0.05}O_3$ and of Ag/2 wt.% CuO for $CaMn_{0.98}Nb_{0.02}O_3$ was used instead of pure Ag paste. Figure 4a presents a cross-sectional profile of the TOM, showing the two K-type thermocouples for ΔT measurements placed on the underside of the upper Al_2O_3 layer (T_{hot}) and on the top side of the bottom Al_2O_3 layer (T_{cold}). Figure 4b and c presents scanning electron microscopy (SEM) pictures of the Al_2O_3–Ag/CuO-p-type leg and Al_2O_3–Ag/CuO-n-type
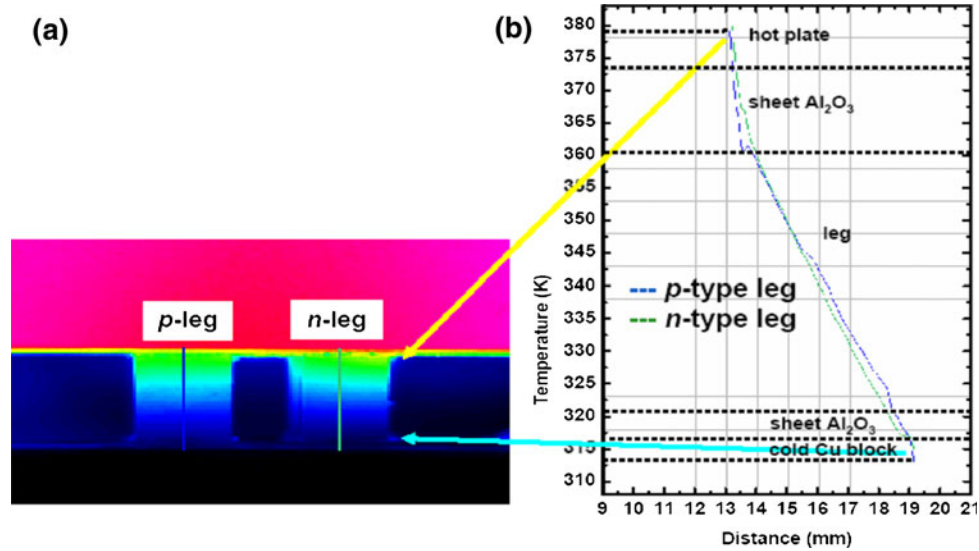
Fig. 5. (a) Temperature distribution in the module measured by a micro-IR camera with T_{cold} = 300 K and T_{hot} = 373 K (T_{cold} and T_{hot} were measured by K-type thermocouples) and (b) analysis of the temperature profile (T as a function of the distance) for p- and n-type legs.

leg cross-sections, respectively. No interpenetration of Ag/CuO particles into the oxide materials was observed. No cracks or gas inclusions were visible by light microscopy in the cross-section, which is a prerequisite for good electrical and mechanical connection. The chosen contact paste compositions were found to improve the mechanical strength of the connection between the Al_2O_3 substrate and the TE elements.

Figure 5a shows the temperature distribution in the module acquired with the micro-IR camera. The temperatures at the cold and hot sides were set to T_{cold} = 300 K and T_{hot} = 373 K, respectively, and measured with K-type thermocouples. Quantitative analysis of the IR picture (Fig. 5b) confirms a nearly linear temperature profile along the surface of the p- and n-type legs. Furthermore, it reveals that the temperatures at the cold and hot sides of the module differ from those measured by the thermocouples attached to the hot plate and to the cooling Cu block. Therefore, the values deduced from the IR picture must be corrected by 8 K. The temperature profile shows significant differences across the alumina substrates on both the hot ($\sim$13 K) and the cold side ($\sim$5 K) of the module. The heat losses, i.e., the difference in the temperature gradients along the legs measured with both methods, have to be taken into account when explaining the divergence between the calculated and measured maximum output power and open-circuit voltage.

The power characteristics were measured for different temperature differences from ΔT = 100 K to ΔT = 500 K. In Fig. 6 it can be seen that the experimental data points of ten different loads fit the typical quadratic form of power source characteristics. The output power increases with increasing temperature gradient as expected. The maximum
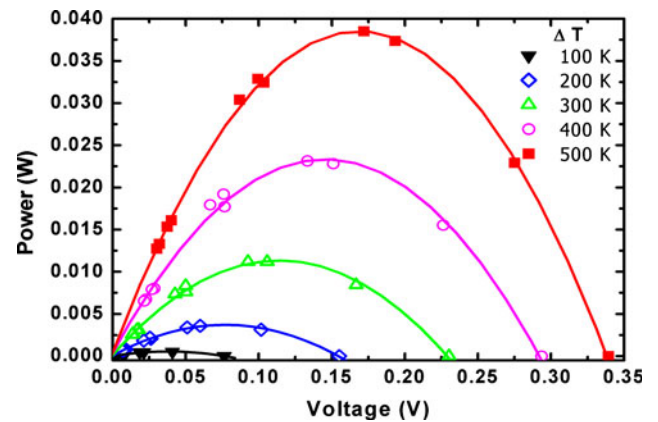

Fig. 6. Power as a function of voltage for various temperature gradients.

output power was evaluated assuming matched loads; inserting $V_{OC}/2$ for V_{load}, formula (2) becomes

$$P_{max} = \left(\frac{V_{OC}}{2R_{in}}\right)^2 \cdot R_{in},\qquad(4)$$

when $R_{load} = R_{in}$.

The maximum output power and open-circuit voltage as a function of temperature difference are plotted in Fig. 7a, together with the internal resistance of the module calculated from Eq. 1. These (experimental) data are compared with the calculated values (Fig. 7b) derived from the measured thermoelectric properties of the p- and n-type materials, assuming a linear temperature profile along the legs as confirmed by the micro-IR camera measurements. The open-circuit voltage was calculated from integrations of the p- and n-type Seebeck coefficient at the same temperature difference (with T_{cold} = 300 K). The resistance of the legs was
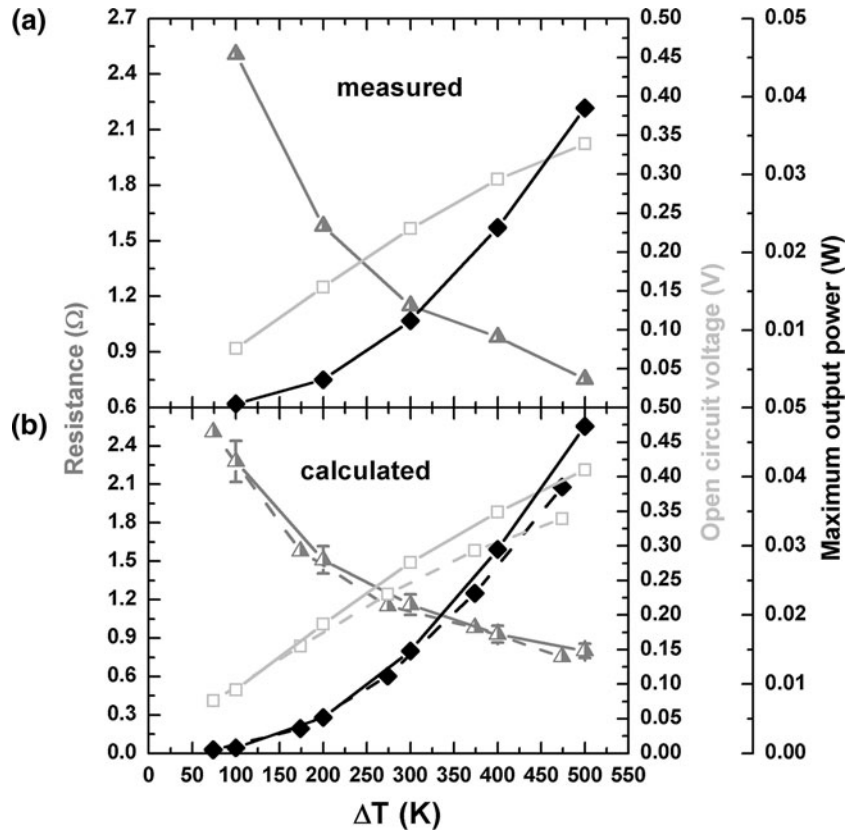
Fig. 7. (a) Maximum output power (*filled symbols*), open circuit voltage (*empty symbols*) and resistance (*half-filled symbols*) evaluated from module measurements and (b) calculated from thermoelectric properties of the *p*- and *n*-type legs. Solid lines are based on temperature measurements by K-type thermocouples and dash lines on temperature gradient analysis by micro-IR camera measurements.

obtained by integrating the resistance of 4 mm $\times$ 4 mm $\times$ 0.1 mm sheets of the *p*- and *n*-type legs over the interval [T_{cold}, T_{hot}]. The integration assumes a linear temperature increment of 10 K, 8 K, 6 K, 4 K, and 2 K for 5-mm legs at temperature differences of 500 K, 400 K, 300 K, 200 K, and 100 K, respectively. At a temperature difference of 500 K, a maximum output power of $\sim$0.04 W was observed. The differences between the measured and the calculated maximum output power can be ascribed to the discrepancy between the calculated and measured open-circuit voltage ($\sim$17% below the theoretical results at $\Delta T = 500$ K), which can be explained by varying temperature values (see above). Taking the IR camera measurements into account, the temperature gradient in the thermo-elements is lower than measured by the thermo-couples. In fact, revision of the temperature characteristics of the resistance, open-circuit volt-age, and maximum output power results in a decrease in the deviation between experimental and calculated data; e.g., the deviation of P_{max} at $\Delta T = 474$ K decreases from 19% to 9% (dashed lines in Fig. 7b).

Based on corrected temperature gradients (dashed lines in Fig. 7b), the measured resistance at $\Delta T = 100$ K is $\sim$2.28 Ω. The resistance calculated from the TE legs resistance is $\sim$2.28 Ω for the same

temperature gradient, which suggests that the value of the contact resistance cannot be estimated due to measurement accuracy (see error bars in Fig. 7b). Accurate determination of the contact resistance at both the hot and the cold joint will be the subject of future work.

CONCLUSIONS

Four-leg thermoelectric oxide modules were pro-duced by combining *p*- and *n*-type thermoelements made of freshly prepared $GdCo_{0.95}Ni_{0.05}O_3$ and $CaMn_{0.98}Nb_{0.02}O_3$, respectively. Both compounds have almost the same thermal conductivity ($\sim$3 $Wm^{-1}K^{-1}$) above 300 K and large thermo-power. The electrical resistivity of the *n*-type material indicates metal-like behavior, whereas the *p*-type material exhibits semiconducting behavior. The quality of the contacts was improved using a mixture of Ag/CuO and TE materials. A thermo-electric module with 5 mm leg lengths was tested under different temperature gradients of ΔT ($T_{hot} - T_{cold}$) up to values of $\Delta T = 500$ K, and the power characteristics were evaluated. The temper-ature gradient through the module was measured by using a micro-IR camera. With this technique, significant temperature gradients between the heat-ing plate and the legs across the alumina substrate

on the hot side ($\sim$18 K) as well as across the alumina substrate on the cold side ($\sim$5 K) were discovered. Measured values of maximum output power ($\sim$0.04 W), open-circuit voltage ($\sim$0.34 V), and resistance ($\sim$0.75 Ω) of the module at ΔT = 500 K were compared with the calculated values of $\sim$0.047 W, 0.41 V, and 0.73 Ω at ΔT = 500 K, respectively. The deviation between the calculated and measured values was mainly caused by the nonideal and underestimated temperature gradient. The limiting factor for the power output is the high module resistance (R_{total} = 2.51 Ω) because of the high contribution of the p-type TE legs resistance. Therefore, the development of an improved p-type material will be a matter of further investigation, as well as the improvement of the contact materials.

ACKNOWLEDGEMENTS

REFERENCES

1. T.-D. Chung, W.-T. Hong, Y.-P. Chyou, D.-D. Yu, K.-F. Lin, and Ch.-H. Lee, *Appl. Therm. Eng.* 28, 933 (2008).
2. S.S. Kim, F. Yin, and Y. Kagawa, *J. Alloys Compd.* 419, 306 (2006).
3. E.S. Reddy, J.G. Noudem, S. Hebert, and C. Goupil, *J. Phys. D: Appl. Phys.* 38, 3751 (2005).
4. W. Shin, N. Muruyama, K. Ikeda, and S. Sago, *J. Power Sources* 103, 80 (2001).
5. R. Funahashi, M. Mikami, T. Mihara, S. Urata, and N. Ando, *J. Appl. Phys.* 99, 066117 (2006).
6. R. Funahashi, I. Matsubara, H. Ikuta, T. Takeuchi, U. Mizutani, and S. Sodeoka, *Jpn. J. Appl. Phys.* 39, L1127 (2000).
7. R. Funahashi, S. Urata, K. Mizuno, T. Kouuchi, and K. Mikami, *Appl. Phys. Lett.* 85, 1036 (2004).
8. J. Hejtmánek, Z. Jirák, M. Maryško, C. Martin, A. Maignan, M. Hervieu, and B. Raveau, *Phys. Rev. B.* 60, 14057 (1999).
9. R. Robert, S. Romer, A. Reller, and A. Weidenkaff, *Adv. Eng. Mater.* 7, 303 (2005).
10. A. Weidenkaff, R. Robert, M.H. Aguirre, L. Bocher, and L. Schlapbach, *Phys. Status Solidi RRL Rapid Res. Lett.* 1, 247 (2007). doi:10.1002/pssr.200701185.
11. A. Weidenkaff, R. Robert, M.H. Aguirre, L. Bocher, T. Lippert, and S. Canulescu, *Renew. Energy* 33, 342 (2008).
12. L. Bocher, M.H. Aguirre, D. Logvinovich, A. Shkabko, M. Trottmann, and A. Weidenkaff, *Inorg. Chem.* 47, 8077 (2008).
13. R. Robert, M.H. Aguirre, P. Hug, A. Reller, and A. Weidenkaff, *Acta Mater.* 55, 4965 (2007).
14. L. Bocher, R. Robert, M.H. Aguirre, S. Malo, S. Hébert, A. Maignan, and A. Weidenkaff, *Solid State Sci.* 10, 496 (2008).
15. A. Weidenkaff, *Adv. Eng. Mater.* 6, 709 (2004).
16. E. Krupicka, A. Reller, and A. Weidenkaff, *Cryst. Eng.* 5, 195 (2002).
17. S. Hébert, D. Flahaut, C. Martin, S. Lemonnier, J. Noudem, C. Goupil, A. Maignan, and J. Hejtmánek, *Prog. Solid State Chem.* 35, 457 (2007).
18. M. Miclau, J. Hejtmánek, R. Retoux, K. Knížek, Z. Jirák, R. Frésard, A. Maignan, S. Hébert, M. Hervieu, and C. Martin, *Chem. Mater.* 19, 4243 (2007).
19. R.M. do Nascimento, A.E. Martinelli, and A.J.A. Buschinelli, *Cerâmica* 49, 178 (2003). ISSN 0366-6913. doi:10.1590/S0366-69132003000400002.
20. H.R. Elsener, J. Janczak-Rusch, V. Bissig, U.E. Klotz, and B. Zigerlig, *Verbundwerkstoffe*, ed. H.-G. Degischer (Weinheim: Wiley-VCH, 2006), pp. 738–743.
21. J.Y. Kim, J.S. Hardy, and K.S. Weil, *J. Am. Ceram. Soc.* 88, 2521 (2005).